Effect of flame characteristics on an isolated ethanol droplet evaporating through stagnation methane/air flames: An experimental and numerical study

Deniz Kaya Eyice, Mehmet Karaca, Fabien Halter, İskender Gökalp, Christian Chauveau

Effect of flame characteristics on an isolated ethanol droplet evaporating through stagnation methane/air flames: an experimental and numerical study

Deniz Kaya Eyice[a,b,c,*], Mehmet Karaca[d], Fabien Halter[a,b], İskender Gökalp[a,e] and Christian Chauveau[a]

[a] *CNRS-INSIS, ICARE, 1C Avenue de la Recherche Scientifique, Orléans, 45071, France*
[b] *Université d'Orléans, Château de la Source, Orléans, 45100, France*
[c] *Dept. of Mechanical Eng., Middle East Technical University, Dumlupınar Bulvarı No. 1, Ankara, 06800, Turkey*
[d] *Dept. of Aerospace Eng., Middle East Technical University, Dumlupınar Bulvarı No. 1, Ankara, 06800, Turkey*
[e] *Clean Energy Technologies, TÜBİTAK MAM, TÜBİTAK Gebze Yerleşkesi, Marmara Araştırma Merkezi, Kocaeli, 41470, Turkey*

ARTICLE INFO

Keywords:
stagnation flame
single droplet evaporation
droplet-flame interaction
Abramzon-Sirignano model

ABSTRACT

A single ethanol droplet evaporation through laminar methane/air stagnation flame is investigated at lean, stoichiometric and rich conditions experimentally and numerically. For the droplets having initial diameters of 20-70 μm, the particle Reynolds number is measured via PIV/PTV, resulting in the slip velocity between the droplet and gas flow being small and the surrounding gas being able to carry without any significant convective effects. Evaporation rates, computed from Abramzon-Sirignano for a moving droplet towards a stagnation flame field, satisfy the ones computed from empirically determined evaporation rates from ILIDS measurements as a function of flame temperature, flame speed and flame thickness. Nevertheless, Abramzon-Sirignano model slightly overestimates the vaporization constant for lean cases. The distance travelled by the droplet after leaving the flame zone determines the average critical diameter. Accordingly, droplets larger than 18 μm can cross the flame, leading to local modifications in the flame region due to heat loss and vapor diffusion from the droplet.

Novelty and Significance

Energy conversion in combustion should be carried out by optimizing efficiency, minimizing pollution, and preventing further climate change. The multiphase nature of spray combustion particularly adds further complexity due to the strong coupling of atomization, evaporation, mixing, turbulence, and chemical reactions. Although spray combustion involves a cloud of polydispersed droplets, it is of fundamental importance to understand the dynamics of an isolated droplet and its interactions with the flame front, which can provide indispensable information for spray combustion models. In this study, an experimental and computational framework has been developed to investigate droplet-flame interactions. The dynamics and evaporation characteristics of an isolated droplets interacting with stagnation flames have been determined by coupling several laser diagnostics, while further enhanced with Eulerian-Lagrangian simulations under flame conditions. Thereupon, the outcomes help the design of injectors of spray combustion systems and enhancement of evaporation models.

Author Contributions

DKE performed research, analysed data and wrote the paper. MK supervised numerical simulations, validated methods/analysis and reviewed the paper. FH supervised research, validated methods/analysis and reviewed the paper. IG supervised research and validated methods. CC supervised research, validated methods/analysis and reviewed the paper.

The publisher version is available using this link :

please cite using the following format :
Kaya Eyice D., Karaca M., Halter F., Gökalp İ. and Chauveau C., Effect of flame characteristics on an isolated ethanol droplet evaporating through stagnation methane/air flames: An experimental and numerical study, [Combustion and Flame], 265, pp. 113465, (2024) doi:https://doi.org/10.1016/j.combustflame.2024.113465

1. Introduction

In combustion applications, liquid fuel is injected into a combustion chamber via an atomization process in which the liquid jet disintegrates into fragments during primary break-up and, finally, into droplets during secondary break-up. Droplet size distribution resulted from the atomization process varies to the application. For combustion in car engines, gas turbines, industrial furnaces, and rocket engines, effective atomization is required to achieve high evaporation and mixing rates since chemical reactions occur at the gaseous phase. Evaporation of droplets and mixing of vaporized fuel with oxidizer directly control the overall energy release rate. In the meantime, presence of liquid fuels in the flame zone has a critical effect on the flame surface at which corrugated structures leads to flame instabilities, hence failure in the application. Therefore, determination of evaporation characteristics for the droplet is essential for engine performance.

Today, with the help of advanced experimental techniques and computational capabilities with efficient numerical methods, understanding of droplet evaporation and its interaction with flame is enhanced. In the literature, there are numerous studies and reviews are available for experimental, theoretical and numerical aspects of the phenomenon (1; 2; 3; 4; 5; 6).

Experimental investigations provide a good database for commonly used liquid fuels and validation of evaporation/combustion models. Several techniques are used to track the evaporation sequence of individual droplets, such as suspension (7; 8), free falling (9; 10), and levitation (11; 12). Laser diagnostics, including Rayleigh scattering, Laser Induced Florescence (LIF), and Interferometric Laser Imaging Droplet Sizing (ILIDS), are also used to measure droplet parameters such as diameter, concentration, and temperature. In diesel engine applications, Rayleigh scattering is coupled with Mie scattering to determine the spray characteristics (13; 14). However, since Rayleigh scattering is shadowed by Mie scattering, simultaneous measurement is impossible for liquid and gaseous phases. Generally, first, the spray parameters are characterized via Mie scattering. Then, the vapor phase is captured with Rayleigh scattering to investigate the evaporation and burning of droplets. Laser Induced Florescence (LIF) is a commonly used technique for combustion applications and the determination of droplet evaporation, especially for spray applications (15; 16; 17; 18; 19). In LIF experiments, the intensity of the fluorescence signal is directly proportional to the molecular density, hence concentration. LIF technique is generally used to determine the temperature change of the liquid phase (20; 21; 22). Another measurement technique relying on the fringe pattern detection of the droplet is Interferometric Laser Imaging Droplet Sizing (ILIDS) (23). Sahu and co-workers used coupled ILIDS, and planar LIF (PLIF) techniques to study evaporation of group droplets and changes in the gaseous phase with acetone droplets (24; 25). In their studies, ILIDS was used to measure the individual droplet size, velocity, and number density in polydisperse sprays, while PLIF data provided vapor concentration distribution to characterize the evaporation. They achieved an effective coupling of ILIDS and PIV for acetone droplets by correcting the droplet center from ILIDS to measure the local vapor concentration with PLIF. Parant et al. also studied coupled Particle Image Velocimetry (PIV) and Particle Tracking Velocimetry (PTV) and ILIDS methods on a counter-current burner with dodecane droplets evaporating through methane/air flame (26). They concluded that it is impossible to detect fringe patterns of the droplets at the zone close to the flame region via ILIDS. To overcome this problem, they introduced a new algorithm to PTV measurement so that the droplets could be followed correctly.

Comprehensive theoretical and numerical studies are carried out to predict the evaporation of a single droplet under various conditions. Firstly, a classical model is proposed by Godsave and Spalding for a liquid droplet evaporating in a stationary gas environment at a fixed temperature and properties, leading to d^2 law (27; 28). Convective heat and mass transfer of an evaporating droplet in the presence of a moving gas has been introduced by correlations in the form of Nusselt, Nu, and Sherwood, Sh numbers. The liquid droplet can be treated as a hard sphere for low mass transfer rates, and the Ranz-Marshall classical convective heat and mass transfer relations are widely used (29). It should also be noted that because the correlations of Nu and Sh numbers account for the effect of relative flow between the droplet and gas, the classic model is applicable when the gas is not stationary but moving relative to the droplet with constant Nusselt and Sherwood numbers. Analytical solutions for the gas phase variables are obtained in quasi-steady evaporation models, and the evaporation rate is calculated. Abramzon and Sirignano improved the classical model by incorporating the Stefan flow effect on the thicknesses of thermal and diffusional films based on film theory by introducing correction factors to Nu and Sh calculations (30). The main assumptions of this model include variable thermophysical properties, infinite thermal conductivity, non-unity Lewis number in the gas film, Stefan flow around the droplet, internal circulation, and transient heating in the liquid phase. Sazhin et al. observed the impact of temperature gradient inside fuel droplets on the evaporation process by comparing the effective and infinite thermal conductivities (31). They reported that temperature gradient within the droplets could significantly reduce

evaporation time by increasing the surface temperature at the preheating phase. Haywood et al. conducted a study for a moving droplet by solving both gas and liquid flow within the droplet (32). They reported that the quasi-steady assumption used in a simplified droplet evaporation model is valid for low Reynolds numbers. Blowing effect due to surface evaporation significantly impacts mass transfer, especially in high evaporation rate cases. Thermodynamic non-equilibrium effects are also considered for the classical model by Miller et al. (33) by introducing Langmuir-Knudsen law and Clausius-Clapeyron law for surface vapor molar fraction calculation.

The interaction between droplets and flame is also widely studied to determine critical design parameters. Most of the studies include spray formation with different burner configurations (34; 35; 36), especially to study the effect of droplets on flame speed (37; 38). The injection of monodispersed droplets is studied to understand the effect of droplet spacing on evaporation. Sangiovanni and Labowsky studied the injection of monodispersed fuel droplets having nearly 100-300 μm diameter into flat flame and recorded the change in droplet surface area (39). They pointed out that while the lifetime of the droplet is consistent with theoretical computations for large droplet spacing, isolated droplets evaporate more than the neighboring droplets. Russo and Gomez studied the effects of droplet and flame parameters on the extinction position of the droplet relative to flame (40; 41). They defined the Damköhler number of vaporization for ethanol droplets as an indication of droplet passage criteria. They also concluded that inter-droplet distance significantly affects the evaporation constant due to the change in vapor properties. Monodispersed ethanol evaporation was also reported by Castanet and co-workers using LIF and PDA for the size, temperature, and velocity of linearly streaming and combusting droplets (42). Orain and Hardalupas also studied monodispersed ethanol injection into premixed natural gas stagnation flame (43). The change in local equivalence ratio is found to depend on the initial droplet size. Mercier and co-workers conducted another study on an isolated acetone droplet and its interaction with methane flame via PLIF (44). It is reported in their study that velocity of the droplet has a major impact on reactivity of the droplet and local flame extinction. They reported that reactivity of the flame front is reduced by the droplet, most likely due to the low vapor temperature generated from the evaporation of the droplet.

In this study, a complementary approach for the evaporation of an isolated ethanol droplet interacting with a laminar methane/air flame is reported. Experimental approach and preliminary experimental results on evaporation were previously reported in Eyice et al. (45; 46). Currently, simulations are also performed under similar conditions via Abramzon-Sirignano model to investigate the evaporation phenomenon, as well as the local changes in the flame field. Droplet passage criteria are defined for ethanol droplets at flame conditions. Evaporation constant is reported in a temperature gradient and empirically correlated to gas temperature and flame parameters. Spalding numbers, heat, and mass evaporation rates are computed at different conditions.

2. Experimental

A stagnation burner is used in this study to observe the interaction of a droplet with a laminar, flat flame. The burner, represented in Figure 1a, consists of a laminarization grid, inner channel for premixed mixture, outer channel for nitrogen co-flow, needle for droplet injection and an upper stabilization plate. Once the premixed mixture of gaseous fuel and oxidizer is fed to the system, a laminar and flat flame can be created by introducing an ignition energy at the region between burner exit and upper stabilization plate. Then, the flame stabilization is enhanced with a nitrogen co-flow. A piezoelectric injector is used to generate monodispersed liquid droplets with nearly 50 μm diameter and they are then fed to the system perpendicularly with a premixed gas flow.

The stagnation burner is coupled with a continuous laser, Coherent Verdi emitting at 532 nm to create a 2D laser sheet for capturing an area perpendicular to the flame. In addition, two high-speed cameras, Phantom v1210 and Phantom v1611, equipped with Sigma APO Macro 180 mm lenses at the maximum opening, are placed crosswise to the flame to observe the scattered light. Visualization of the flame front and temporal monitoring of the droplet evaporation are performed using planar laser tomography. Mie scattering is utilized to determine the position of the flame front and velocity of unburnt gases via Particle Image Velocimetry (PIV) and the velocity of the droplet via Particle Tracking Velocimetry (PTV). In addition, Interferometric Laser Imaging for Droplet Sizing (ILIDS) is coupled with Mie scattering to obtain droplet size variation during evaporation. Details of the experimental setup, diagnostics and post-processing approaches can be found in Eyice et al. (46).

Flame field computations are performed in Cantera (47) to determine the flow and flame field characteristics of the experimental conditions. Accordingly, 1D stagnation flame is computed using multi-species transport with the San Diego mechanism containing 57 species and 268 reactions (48). In this configuration, the flame is stabilized in a strained flow field at an axisymmetric stagnation point with the presence of a stabilization plate. The location at

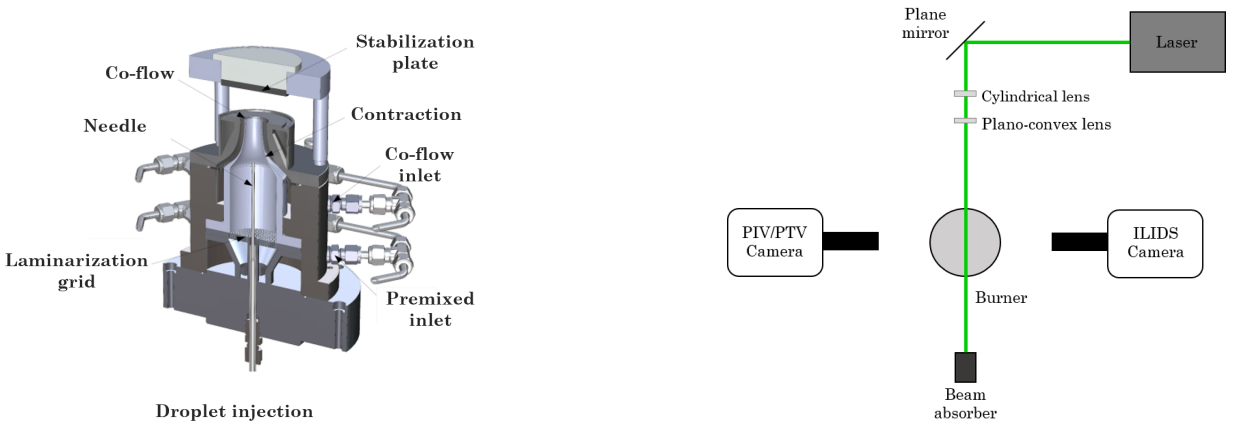

Figure 1: (a) Schematic of the flat flame burner (b) Experimental configuration (46)

which the flame is stabilized depends on unburnt gas velocity, U_0 and stagnation plate temperature, T_{plate}. Since the stagnation plate temperature is not measured experimentally, first, sensitivity of flame temperature to plate temperature is studied. Accordingly, for plate temperature ranging between 300-1500 K, flame temperature is changing nearly by ± 2 K. Since injected droplets are evaporating in the burnt gases and cannot reach the plate, the plate temperature is assumed to be constant at 500 K for all computed cases.

Experiments are performed with an ethanol droplet and methane/air premixed flames at the conditions given in Table 1. For each sequence of experiments, individual droplets are selected over all recordings, and the complete post-processing of PIV/PTV and ILIDS is performed for each droplet to track its evaporation.

Table 1: Parameters of 1D stagnation CH_4/air flames at 300 K, 1 atm (T_{plate}=500 K and U_0) computed with the San Diego mechanism (48)

Condition	ϕ	U_0 (m/s)	S_L (m/s)	T_f (K)	δ_L (μm)
SBM-1	0.8	0.560	0.303	1991.6	527
SBM-2	0.9	0.743	0.364	2123.2	481
SBM-3	1.0	0.824	0.394	2212.2	469
SBM-4	1.1	0.699	0.379	2202.4	474

3. Numerical

Computations are performed with YALES2 solver, based on finite volume method for low Mach number flows with variable density simulation (49). The solver implements Eulerian-Lagrangian approach to solve two-phase flows in which a droplet is considered as an isolated point in Lagrangian frame. A two-way coupling approach transfers mass, momentum and energy from the liquid phase to the gas phase via source terms.

In the Eulerian-Lagrangian approach, the liquid phase is defined as the Lagrangian flow elements, which are assumed to be rigid spheres and spatial points submerged in the surrounding gaseous phase. Mass of the particle can be computed directly from:

$$m_p = \rho_p \frac{\pi}{6} d_p^3 \tag{1}$$

where m_p, ρ_p and d_p are mass, density and diameter of the particle. Trajectory, $\mathbf{x}_p$ and momentum, m_p $\mathbf{u}$ of the particles are calculated at the corresponding spatial location:

$$\frac{d\mathbf{x}_p}{dt} = \mathbf{u}_p \tag{2}$$

$$\frac{dm_p\mathbf{u}_p}{dt} = \mathbf{F}_p^{ext} \tag{3}$$

where $\mathbf{u}_p$ is velocity of the particle and $\mathbf{F}_p^{ext}$ represents the external forces acting on the particle, which includes gravitational $\mathbf{F}_G$ and the aerodynamic $\mathbf{F}_A$ forces. Gravitational forces, $\mathbf{F}_G$ can be defined as:

$$\mathbf{F}_G = (\rho_p - \rho)\frac{\pi}{6}d_p^3\mathbf{g} \tag{4}$$

where ρ is density of the carrier gas and $\mathbf{g}$ is the gravitational acceleration.

Aerodynamic forces are mainly drag and pressure forces. Under a constant pressure environment, only drag force is considered:

$$\mathbf{F}_A = m_p\frac{1}{\tau_p}(\mathbf{u}_p - \mathbf{u}_\infty) \tag{5}$$

where $\mathbf{u}_\infty$ is velocity of the carrier gas and τ_p is relaxation time:

$$\tau_p = \frac{4}{3C_D Re_p}\frac{\rho_p}{\rho}\frac{d_p^2}{\nu} \tag{6}$$

where ν is kinematic viscosity of the carrier gas and Re_p is the particle Reynolds number, is also defined as:

$$Re_p = \frac{d_p|\mathbf{u}_p - \mathbf{u}_\infty|}{\nu} \tag{7}$$

Drag coefficient, C_D can be computed from Shiller and Nauman emprical correlation (50) for $Re_p < 1000$:

$$C_D = 24(1 + 0.15Re_p^{0.687}) \tag{8}$$

The vaporating particles contribute to the Eulerian conservation equations that govern the gaseous phase via source terms; mass, Θ_M, momentum,Θ_D and energy, Θ_H:

$$\Theta_M(\mathbf{x},t) = \frac{1}{\Delta V}\int_{\Delta V}\sum_{n=1}^{N_p} -\dot{m}_p^{(n)}\delta\left(\mathbf{x} - \mathbf{x}_p^{(n)}(t)\right)dV \tag{9}$$

$$\Theta_D(\mathbf{x},t) = \frac{1}{\Delta V}\int_{\Delta V}\sum_{n=1}^{N_p} -\mathbf{F}_p^{(n)}\delta\left(\mathbf{x} - \mathbf{x}_p^{(n)}(t)\right)dV \tag{10}$$

$$\Theta_H(\mathbf{x},t) = \frac{1}{\Delta V}\int_{\Delta V}\sum_{n=1}^{N_p}\left(m_p^{(n)}C_p\frac{dT_p^{(n)}}{dt} + \dot{m}_p^{(n)}L_v\right)\delta\left(\mathbf{x} - \mathbf{x}_p^{(n)}(t)\right)dV \tag{11}$$

where ΔV is the control volume of mesh cell containing the droplet n, C_p is specific heat of the particle, T_p is temperature of the particle, $\dot{m}_p$ is mass flowrate of the particle and L_v is latent heat of vaporization.

3.1. Evaporation model

The temperature difference between the liquid and gaseous phases leads to the evaporation of a droplet meaning heat and mass transfer between the two phases. First, the droplet is heated through conduction from the gaseous phase, which increases the internal energy of the droplet's molecules. Hence, the molecules detach from the droplet, and vapor concentration increases near the droplet surface. Because of the high concentration gradient, mass is transferred from the droplet's surface to the gaseous phase. Consequently, the evaporation rate is defined as the diffusion rate of the liquid from the droplet's surface to the surrounding gas. The simplest model for evaporation is proposed by Spalding (27). Later, Abramzon and Sirignano extended the evaporation model by accounting for the effects of convective flow around the droplet (30).

The main assumptions of the evaporation model can be listed as (27):

– The droplets are perfectly spherical and dispersed.

– Thermal conductivity of the droplet is infinite, and the temperature of the droplet, T_p is constant.

– At the liquid/gas interphase, a thermodynamic equilibrium exists between the surrounding gas and the droplet. Therefore, using the Clasius-Clapeyron relation, it is possible to determine the partial saturated vapor pressure, P_s at the droplet surface:

$$P_s = P_{ref} \exp\left[\frac{W\, L_v}{R}\left(\frac{1}{T_{evap}} - \frac{1}{T_p}\right)\right] \tag{12}$$

where W is molar mass, T_{evap} is evaporation temperature of the droplet at the reference pressure, P_{ref}=1 atm and R is the gas constant.

– Thermal diffusivity of the droplet, $\mathcal{D}$ is lower than thermal diffusivity of gas. Therefore, thermal response is quasi-stationary in the gaseous phase.

– The properties of the surrounding gas remain unchanged from the droplet surface to the far-field. These properties are calculated from the 1/3 law proposed by Hubbard (51):

$$T_{1/3} = \frac{2}{3}T_s + \frac{1}{3}T_\infty \tag{13}$$

$$Y_{1/3} = \frac{2}{3}Y_s + \frac{1}{3}Y_\infty \tag{14}$$

where T and Y are temperature and mass fraction of the carrier gas, respectively. Subscript s denotes the surface values of mass fraction of the droplet, Y_s and temperature, T_s. While subscript ∞ denotes the far-field values of evaporated mass fraction, Y_∞ and temperature, T_∞.

– The liquid phase is an ideal mixture, and no chemical reaction takes place.

– The solubility of the ambient gas in the liquid is negligible.

– The effects of gravity and radiation are negligible.

Droplet mass temporal evolution is determined assuming the fuel mass flux leaving the droplet surface equal to the variation of mass of the droplet:

$$\frac{dm_p}{dt} = \dot{m}_p = -\pi\, d_p\, Sh\, \rho_p\, \mathcal{D}\, ln(1 + B_M) \tag{15}$$

where Sh is the Sherwood number, $\mathcal{D}$ is the diffusion coefficient and B_M is Spalding mass number which characterizes the effect of mass transfer and is defined as:

$$B_M = \frac{Y_s + Y_\infty}{1 - Y_s} \tag{16}$$

Using the relation of mass variation, the change in droplet diameter is expressed as:

$$d_p^2 = d_{p,0}^2 - \frac{8\rho\mathcal{D}}{\rho_p} ln(1 + B_M)t = d_{p,0}^2 - Kt \tag{17}$$

where $d_{p,0}$ is initial diameter of the droplet. Equation 17 is also known as d^2 law from which the evaporation rate, K can directly be calculated.

Temporal evolution of the droplet temperature is estimated by integrating the energy equation from the droplet surface to the far-field:

$$\frac{dT_p}{dt} = \frac{\dot{m}_p}{m_p\, C_p}\left[\frac{C_{p,ref}}{B_T}(T_s - T_\infty) + L_v\right] \tag{18}$$

where B_T is the Spalding heat number defined as:

$$B_T = (1 - B_M)^{\frac{Sh\,Pr}{Nu\,Sc}} - 1 \tag{19}$$

where Pr is the Prandtl number, Sc is the Schmidt number. Sh and Nu are the Sherwood and Nusselt numbers, respectively and they are computed using the Ranz-Marshall correlation (29):

$$\begin{aligned} Sh &= 2 + 0.6 {Re_p}^{1/2} Sc^{1/3} \\ Nu &= 2 + 0.6 {Re_p}^{1/2} Pr^{1/3} \end{aligned} \tag{20}$$

Convective flow around the droplet creates a boundary layer and increases mass and heat transfer, hence, the evaporation rate.

To introduce the effect of the laminar boundary layer surrounding the droplet, Abramzon and Sirignano proposed a correction function, F for Sh and Nu numbers as (30):

$$\begin{aligned} F_{M/T} &= 1 + {B_{M/T}}^{0.7} \frac{\ln(1 + B_{M/T})}{B_{M/T}} \\ Sh^* &= 2 + \frac{Sh - 2}{F_M} \\ Nu^* &= 2 + \frac{Nu - 2}{F_T} \end{aligned} \tag{21}$$

3.2. Computational domain

In order to investigate droplet behavior interacting with a flame, a droplet is injected through a 2D stagnation flame field. The computational setup is represented in Figure 2. Domain size is determined based on the burner configuration, at which 25 mm is the distance from the burner exit to the stagnation plate and 15 mm is the diameter of the premixed inlet chamber at the burner exit. Cartesian grid is resolved uniformly at 200 μm.

Flame is initialized using previously computed 1D freely propagating adiabatic flame field, and the initial position of the flame is determined based on Cantera simulations. Unburned premixture is injected from the bottom boundary at conditions corresponding to the experiment. The wall temperature at the upper boundary is fixed at 500 K. Outlet flow conditions are defined on the right and the left boundaries. Depending on the case, 2D flame field computations are carried out until a steady state solution is attained using a CFL value of 0.4, which is achieved at some point within 4000-7000 iterations. The maximum value of the CH_3 species profile is used for determining the flame position.

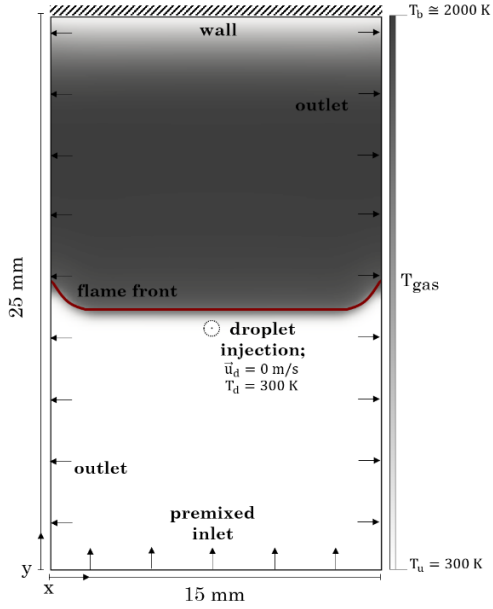

Figure 2: Computational domain of 2D CH_4/air stagnation flame (SBM-1, T_{plate}=500 K)

An isolated ethanol droplet is injected into the steady 2D flame field at T=300 K without an initial velocity. In order to preserve the sphericity of the droplet, 3rd dimensional distance is set to 15 mm along the z-direction. The initial position of the droplet is set at 1.5 mm below the flame position so that the droplet is injected within the unburned premixture having sufficient time to be entrained by the gas flow. The initial droplet diameter is set to 35, 50, and 65 μm for each case to allow a comparison with the different experimental cases. The evaporation of the droplet is followed until complete evaporation using the Abramzon-Sirignano model. During the evaporation process, changes in the droplet parameters, as well as the gas properties, are calculated.

4. Results

4.1. Evaporation through laminar CH_4/air flame

In Figure 3, velocity profiles of the unburnt gases of a stoichiometric flame measured up to the T=525 K isotherm via PIV and ethanol droplet with an initial diameter of 50 μm measured via PTV, as well as the computed profiles, are reported. Alignment of the experimental and numerical data is achieved thanks to T=525 K isotherm.

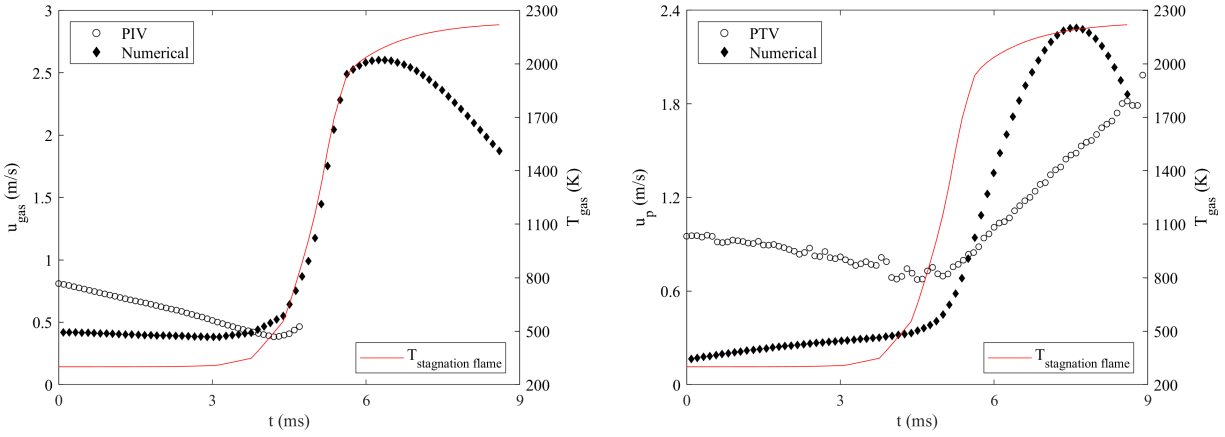

Figure 3: Temporal evolution of computed and measured (a) gas and (b) droplet velocities at SBM-3 ($d_{p,0}$=50 μm)

Flame region detection is achieved experimentally by seeding DEHS droplets into unburnt gases. Since DEHS droplets evaporate at T=525 K, it is not possible to detect the entire flame region with this method. Instead, flame front is defined experimentally based on T=525 K isotherm. The isotherm is resolved from the overlay of 100 images to have more accuracy. Then, temperature profile of the flame is interpolated to the experimental field based on this isotherm. Additionally, no wall reference is recorded for the burner outlet leading to differences between experiments and computations, especially at the first detection location of DEHS droplets. It can still be concluded that PIV measurements provide reliable data, especially near the flame zone. The lowest velocity before the flame region, which is accepted as the flame speed for stagnation flames, is measured as 0.383 m/s via PIV, while numerically, it is computed as 0.389 m/s for SBM-3. Considering other flame conditions, flame speed can be reported with an average difference of 2$\pm$0.5 % between the experiments and computations. It should also be noted that the presence of DEHS droplets ($\approx$ 2-3 μm) does not have an effect on the gas velocity measurements (52).

Figure 3b shows the temporal change of droplet velocity while traveling through the flame field. The first detection of the droplet is achieved after a certain distance from the burner outlet and this position differs for each measured droplet in the whole experimental campaign. Since no wall reference can be captured due to magnification arrangement, it may not be accurate to report the exact initial location of the droplet relative to the flame zone and burner outlet. However, in the numerical simulations, the initial position of each droplet should be assigned such that the droplet is injected from unburnt gases having enough time to be carried by the gas flow. In order to eliminate the effect of the initial droplet position in the simulations, all droplets are injected at a point 1.5 mm below the flame position for all computed cases. Therefore, initial droplet velocity differs in experimental and numerical results.

As soon as the droplet enters the flame region, it accelerates due to the loss of mass; hence, it is subject to less drag force. The relative velocity between gas and liquid phases also directly affects the motion of the droplet, in addition to the evaporation rate. Hence, convection around the droplet and the Marangoni effect at the interface are critical to correctly predict local and global evaporation rates. For all the droplets having an initial diameter between 20-70 μm, the slip velocity between the droplet and unburnt gas is calculated to be negligibly small at the performed flame conditions. Stokes number, St characterizes this effect as being the ratio of characteristic time of the droplet to characteristic time of the gas:

$$St = \frac{\tau_p}{\tau_g} = \frac{\frac{\rho_p {d_p}^2}{18\mu}}{\frac{\delta_L}{\mathbf{u}_\infty}} \tag{22}$$

where μ is dynamic viscosity of the carrier gas and δ_L is the flame thickness.

Under the reported flame conditions, characteristic time of droplets, having an initial size in the range of 20-70 μm, is much lower than that of gas; hence St is below one. Therefore, it can be concluded that droplets are small enough to be carried by gas flow. In order to support the dynamic characteristics of the droplets having a size greater than 5 μm and St greater than 0.1, particle Reynolds number, Re_p is also computed and its temporal evolution is reported in Figure 4 for the stoichiometric flame and 50 μm droplet.

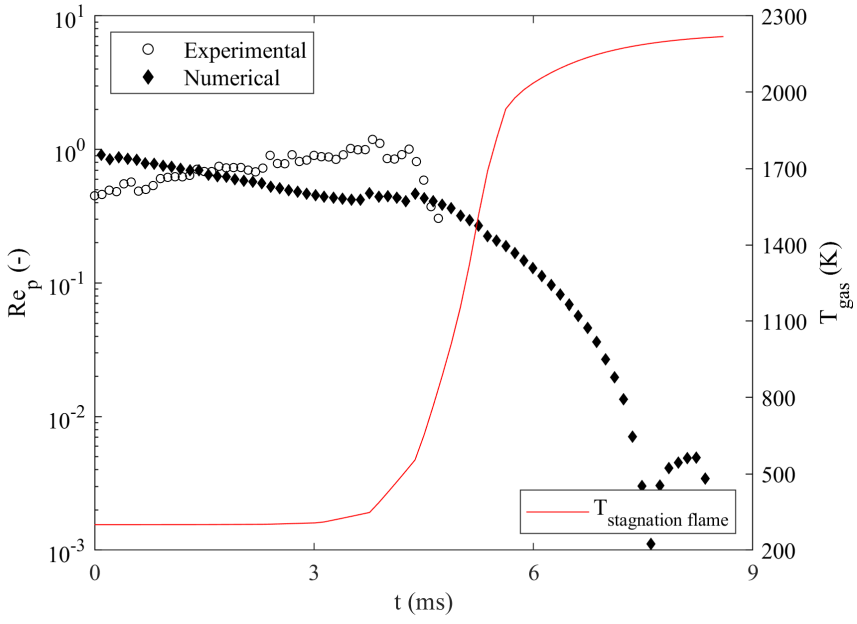

Figure 4: Temporal evolution of particle Reynolds number at SBM-3 ($d_{p,0}$=50 μm)

It is seen that through the entire domain, Re_p value is below 0.1 for all droplets demonstrating that the convective effects from the surroundings are inconsequential for the droplet. Although the relative velocity is higher at the burnt gases, Re_p decreases due to the increase in gas density and viscosity.

Figure 5 shows spatial and temporal evolution of an ethanol droplet diameter subjected to stoichiometric methane/air flame. It is seen that during the initial 8 ms, the droplet moves towards the flame front at a constant size since the ambient temperature is 300 K. Initial heating period is observed for the following 1 ms at the region where the diameter evolution profile starts to create a slope smoothly. The last phase, between 9-13 ms, is the evaporation of the droplet, obeying the d^2 law.

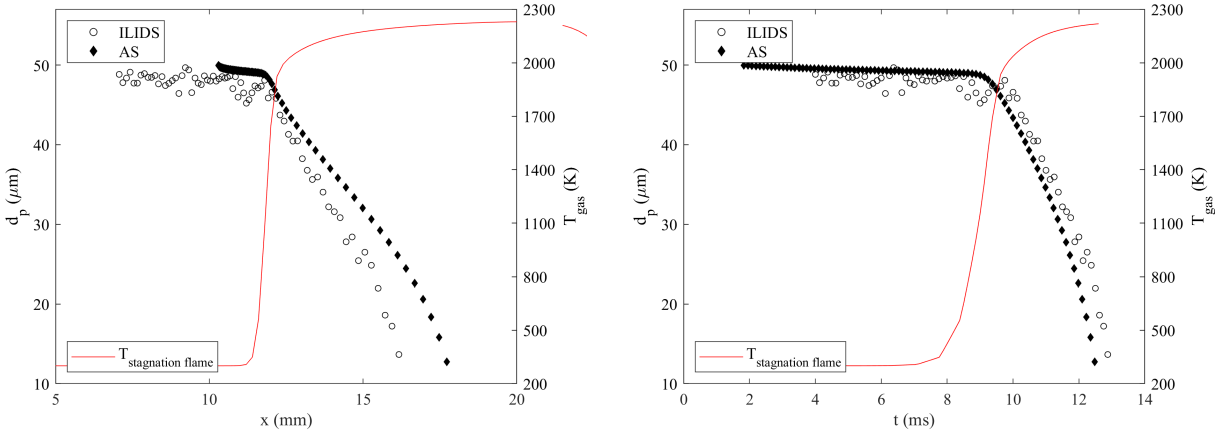

Figure 5: (a) Spatial and (b) temporal evolution of droplet diameter with ILIDS and Abramzon-Sirignano (AS) model at SBM-3 ($d_{p,0}$=50 μm)

As it is seen from the Figure 5a, the simulations reveal a 10 % overestimation of the final droplet location due to differences in the droplet's initial position, although almost identical trend is observed. First of all, experimentally, initial position of the droplet is detected via PTV, and the exact distance between the droplet and flame may slightly differ for each droplet depending on the initial size and detection time. However, for the simulations, the droplet is injected without an initial velocity from 15 mm below the flame zone for all flame conditions. This situation will cause differences in the drag force acting on the droplet due to the variations of droplet and gas velocity. At the initial phases, gas velocity will be higher than velocity of the droplet up to almost 5 ms, as seen from Figure 3. After this time, velocity of the droplet will always be lower than the gaseous phase. It should also be mentioned that as the droplet becomes smaller, it may be trivial to capture the effect of gaseous phase on the droplet in the simulations due to constant grid size. Therefore, detailed tuning may be required to the computations of droplet dynamics in the Abramzon-Sirignano model as the droplet shrinks. Nonetheless, temporal evolution of the droplet, given in Figure 5b is well captured numerically.

Figure 6 shows changes in droplet temperature and Spalding numbers, as well as the mass and heat evaporation rates at stoichiometric conditions for three different particle sizes. Evaporative properties are linearly increasing with the initial droplet diameter, as expected. The overall pattern of all curves shows that as the droplet enters the flame region, heat transfer from the surrounding gas helps to heat the droplet rather than vaporizing and as a result, the droplet temperature rises until it reaches the wet-bulb temperature. Once the droplet reaches the wet-bulb temperature, it begins to create vapor. As the droplet temperature is constant, the mass evaporation rate decreases indicating that the vaporization process started. The largest droplet heats more quickly than the others since it is exposed to higher temperatures for a longer time inside the flame region. The slope of mass transfer rate at the early stages of the vaporization is comparably the same for all droplet sizes since the process is mainly governed by the surrounding temperature at this stage. However, the largest droplet spends more time in the reaction zone which slightly increases its evaporation rate by 0.01 mm^2/s, as it is seen from the mass and heat evaporation rates.

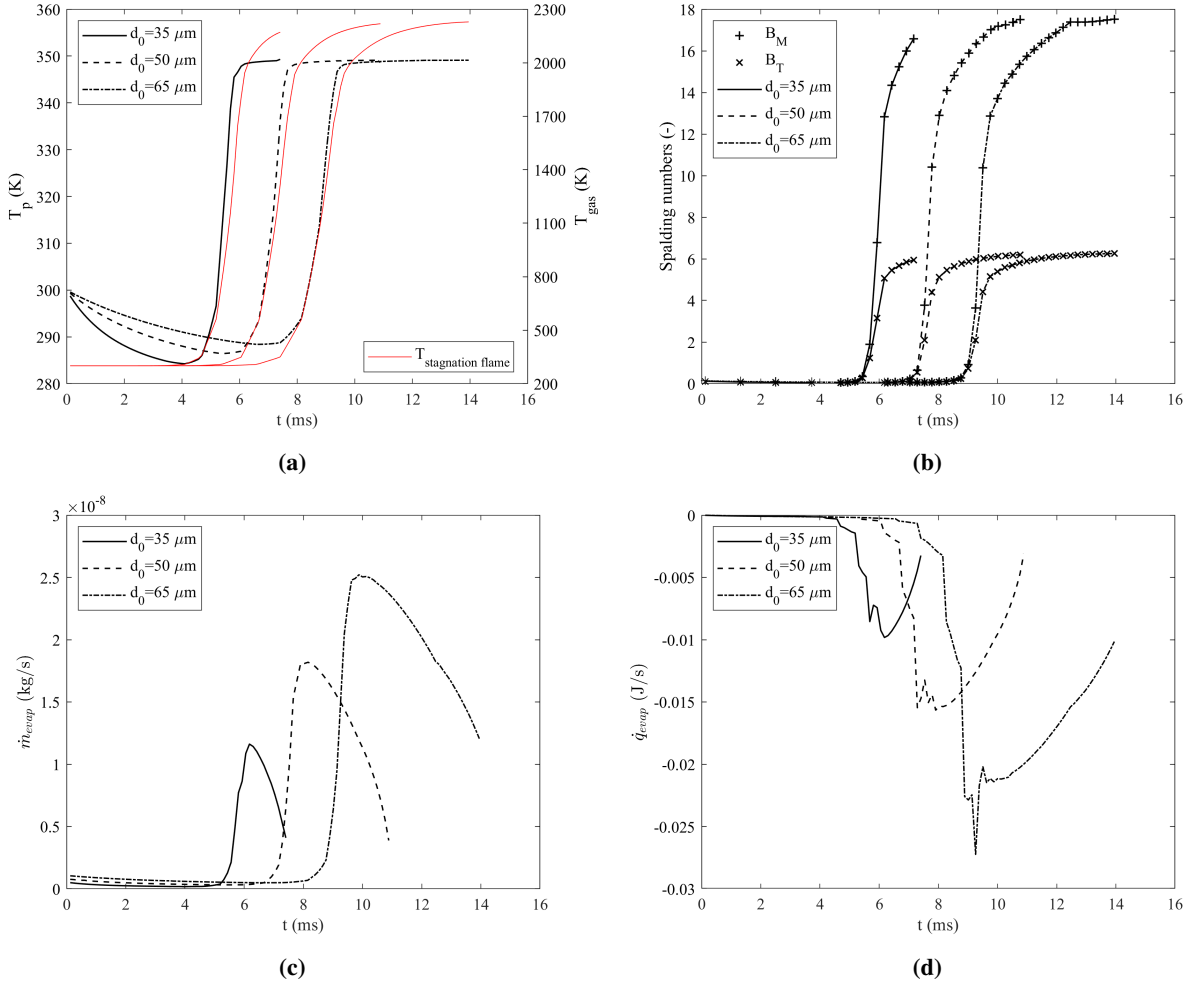

Figure 6: Temporal evolution of droplet parameters at stoichiometric conditions for an ethanol droplets having $d_{p,0}$=35, 50 and 65 μm (a) Droplet temperature (b) Spalding numbers (c) Mass evaporation rate (d) Heat evaporation rate

The effect of flame condition on the evaporative properties of an ethanol droplet is reported in Figure 7. Droplet temperature increases until the boiling temperature of ethanol, nearly 351 K, and the droplet spends most of its time inside the preheating zone while heating. The droplet heating period is almost similar at the performed flame conditions, except that at ϕ=0.8, almost 2 ms delayed is observed. Lower gas/flame velocity leads to lower droplet velocity at this condition, hence the heating of the droplet delays. The increased convective flow with the increased flame speed at ϕ=0.9, 1.0 and 1.1 results in larger B_M and B_T causing more rapid temperature changes in the region close to the droplet. Although the mass evaporation rates are comparable, lower evaporation rate is observed for the droplet exposed to the leanest flame condition. While the overall changes in mass and heat evaporation rates of the droplet can be observed in Figures 6c, 6d, 7c and 7d, local effects and the interrelation between the droplet and flame will be discussed in Section 4.4 in details.

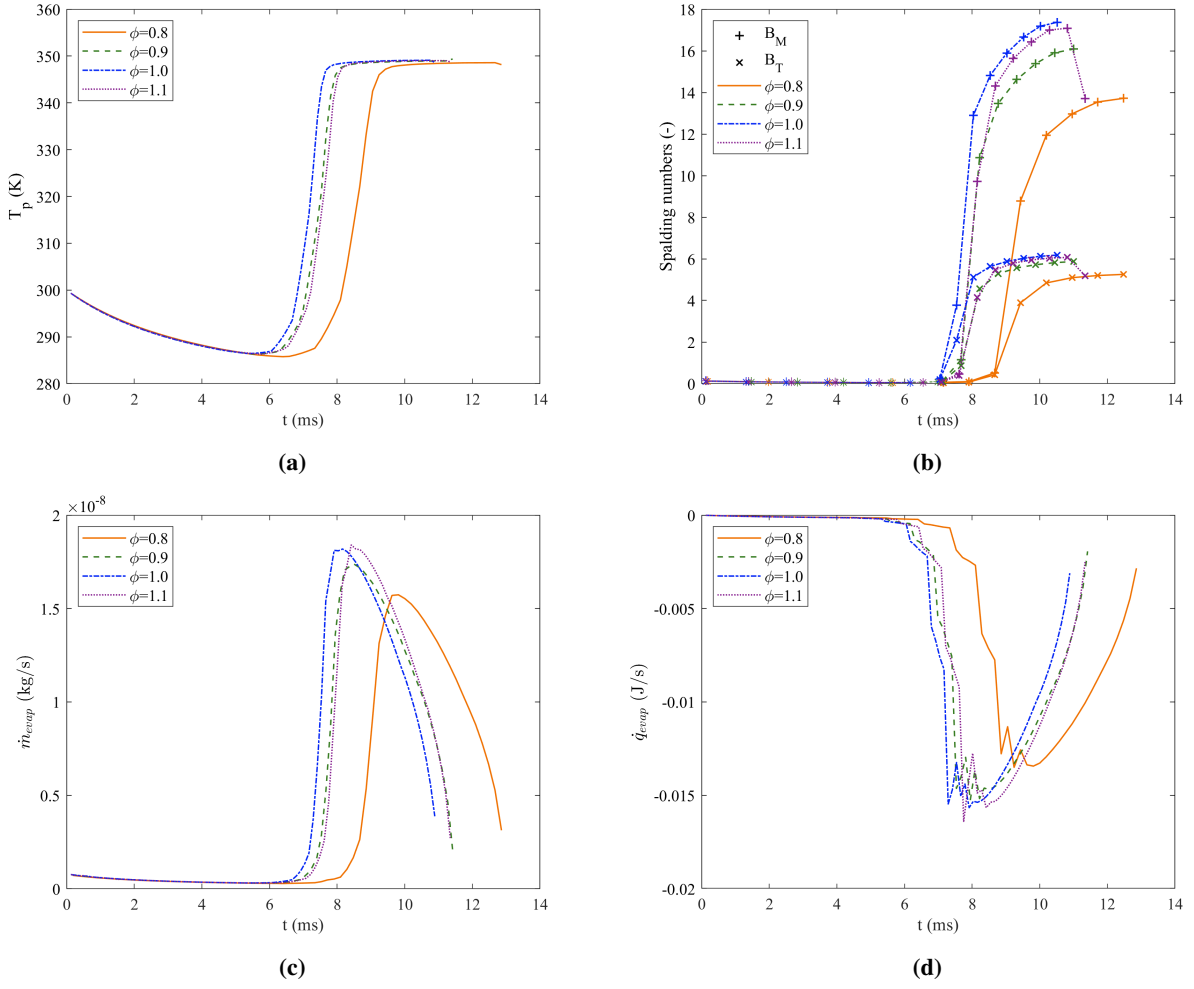

Figure 7: Temporal evolution of droplet parameters at different flame conditions for an ethanol droplet having $d_{p,0}$=50 μm (a) Droplet temperature (b) Spalding numbers (c) Mass evaporation rate (d) Heat evaporation rate

4.2. Rate of evaporation

Following the d^2 law for evaporation rate, K, slope of d^2 vs. t is computed over the diameter change interval for all recorded droplets having initial diameters between 20-70 μm. Although the variability of the initial diameter provides a good database for the evaporation constant, instead of selecting some droplets, mean values of K, mean interval temperature, minima, and maxima to report the evaporation temperature range are computed and given in Figure 8 over all samples at each equivalence ratio, indicated as ILIDS. Experimental results are compared with the literature (Saharin et al. (53)) and previously computed stationary droplet evaporation with Spalding model (45; 46) and a moving droplet through the stagnation flame field computed with Abramzon-Sirignano model (AS).

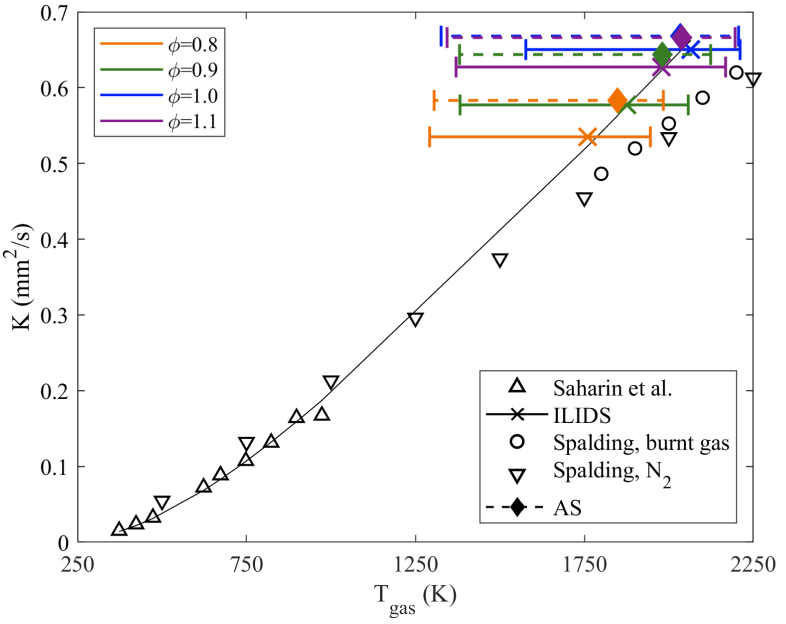

Figure 8: Comparison of ethanol evaporation constant with respect to ambient gas temperature

For stationary droplets, evaporation computations are performed via the Spalding model at each equivalence ratio at the ambient temperatures varying between 1800-2200 K and at the burnt gas compositions (45). Since the mass fraction of a single ethanol droplet is very small in comparison with the major species of methane/air flame including CH_4, CO_2, H_2O, the evaporation constant is computed to be the same for stationary ambient cases. Hence, it is clearly seen that the ambient gas composition has no significant effect on evaporation under evaluated conditions.

Evaporation of the droplet is observed in the flame zone at which the droplet diameter constantly decrease inside a very steep temperature profile. Therefore, it is not possible to report a single evaporation temperature for a moving droplet. Accordingly, evaporation temperature is calculated as the mean temperature in an interval where the droplet starts evaporating and its lifetime ends. It is seen that the maxima of the measured evaporation constants are very close to the numerical results obtained from both Abramzon-Sirignano and Spalding models. Also, Abramzon-Sirignano model slightly overestimates the vaporization constant for lean cases while the values are still in the trend of experimental measurements.

In order to investigate the dependence of the evaporation constant to the ambient temperature, an exponential type of relationship can be used due to rapid growth at low temperatures with the asymptotic behavior, as it can be seen in Figure 8:

$$K(T_{gas}) = AT_{gas}^{\beta} exp(-E_a/RT_{gas}) \tag{23}$$

Table 2: Coefficients of the relation for evaporation constant, K as a function of T_{gas}

A	β	E_a
7.9x10^{-4}	0.947	8429 J/mol

Table 2 reports the fitted values to the Equation 23 from the experimental results. However, it can be clearly seen from Figure 8 that K is not only a function of ambient gas but also changes depending on the flame properties. Moreover, it is hard to report the exact gas temperature for a moving droplet through the ambient with a varying temperature. Hence, it would be beneficial to estimate the vaporization rate depending on flame characteristics which are the parameters such as flame speed, flame temperature etc. depending on fuel-to-air ratio, as well as the species of

fuel and oxidizer. Accordingly, a new Arrhenius type of relation is proposed by introducing flame thickness, δ_L, flame speed, S_L, and flame temperature, T_f, as in Equation 24:

$$K(T_f, S_L, \delta_L) = A' \left(\frac{\delta_L}{S_L} \right)^{\gamma} T_f^{\beta} exp\left(\frac{-E_a}{RT_f} \right) \tag{24}$$

Table 3: Coefficients of the relation for evaporation constant, K as a function of flame parameters

A'	γ	β	E_a
8.9x10^{-4}	0.030	0.947	8429 J/mol

While the activation energy, E_a and the power dependence of temperature, β are kept constant, it is seen that the fitted parameters provide very close computations of evaporation constant for ethanol droplet evaporating through methane/air flame field at ϕ=0.8-1.1. Additionally, the small value of γ indicates that the evaporation constant slightly depends on the characteristic flame time and the ratio of flame thickness to flame velocity. The main governing parameter on evaporation can be interpreted as the flame temperature.

4.3. Droplet passage criteria

Determination of whether the droplet can cross the flame or not is essential in terms of the prediction of instabilities. If droplets evaporate before entering the reaction zone, purely gaseous phase combustion will occur. However, the presence of droplets in the reaction zone causes different modes of combustion depending on the physical properties of the droplet and gaseous flame, leading to local extinctions on the flame surface and hydrodynamic instabilities (54). In this scope, passage criteria for the droplet are defined depending on the initial droplet size.

Damköhler number for vaporization, Da_v is defined as the ratio between evaporation characteristic time, τ_{ev} and preheating time of the flame, τ_f as (55):

$$Da_v = \frac{\tau_{ev}}{\tau_f} = \frac{\frac{d_0^2}{K}}{\frac{\delta_L}{S_L}} \tag{25}$$

For Da_v<1, droplets will completely evaporate inside the flame, while for Da_v>1, longer evaporation time will be observed so that the droplets will cross the flame region. In Figure 9, computed Da_v for all droplets are given. It is seen that at the performed conditions, all droplets evaporate in the burnt gas region.

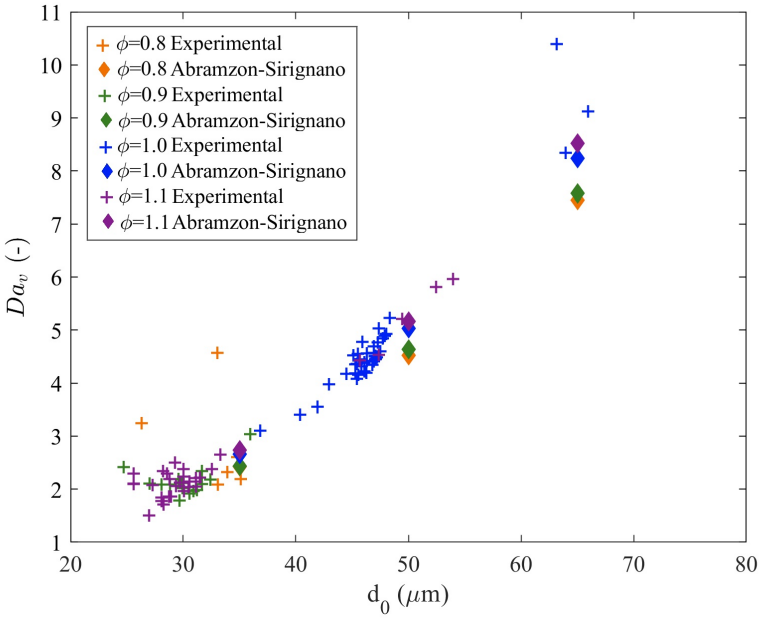

Figure 9: Computed Da_v numbers for all droplets

Accordingly, critical diameter for the droplet, $d_{critical}$ to cross the flame region is defined with two approaches. First of all, with the assumption that all the droplets reaching the flame have equal average vaporization constant, $d_{critical}$ can be computed as a function of residence time in the flame (41):

$$d_{critical,Da_v} = \sqrt{\frac{\bar{K} S_L}{\delta_L}} \tag{26}$$

where $\bar{K}$ is the average evaporation constant at the flame condition.

The second approach includes the direct relation of the distance traveled by the droplet from T=525 K isotherm to its last position depending on the initial droplet size at all flame conditions, given in Figure 10. Since the initial position and velocity may differ for each droplet, a criterion is defined after the droplet enters the flame zone. As it is seen from the figures, at ϕ=1.0, three droplets having an initial diameter greater than 65 μm are reported. As the general trend is observed, these droplets can be considered as outliers. Additionally, Da_v involves the square of the droplet diameter. The same inaccuracy in diameter measurement will therefore lead to greater variability at larger diameters.

Extrapolation is performed to determine the critical diameter, $d_{critical,exp.}$ and $d_{critical,num.}$ reported in Table 4 below such that $\Delta x_{flamecross}$ equals to zero. Hence, if $d_{p,0} < d_{critical}$, the droplet evaporates before reaching the reaction zone while for $d_{p,0} > d_{critical}$, the droplet can cross the flame front.

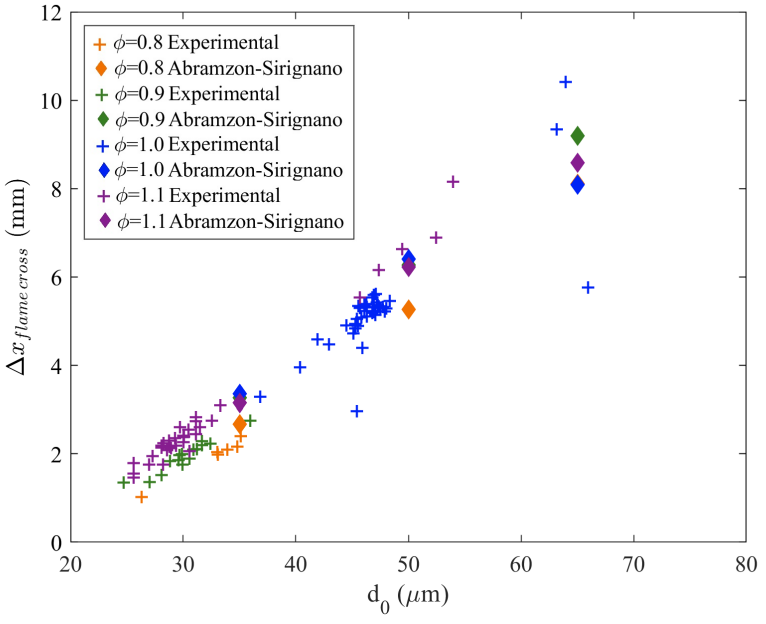

Figure 10: The distance at which the droplet passes after entering the flame zone (T=525 K) for all droplets

Table 4: Critical diameter values of ethanol droplets to cross the flame zone

Condition	ϕ	$d_{critical,exp.}$ (μm)	$d_{critical,num.}$ (μm)	$d_{critical,Da_v}$ (μm)
SBM-1	0.8	19.39	20.50	22.27
SBM-2	0.9	16.05	18.37	21.87
SBM-3	1.0	18.16	12.03	21.85
SBM-4	1.1	18.71	16.91	21.17

As it is seen from Table 4 that the average critical diameter is experimentally found to be 18±1.3 μm for ethanol droplet from the direct measurement of distance travelled by the droplet. However, the critical diameter computed from the Abramzon-Sirignano model slightly differs from the experiments. At stoichiometric condition, it is underestimated with an error of 33 %. This can be explained mainly due to the fact that the highest temperature is observed at this condition, leading to a lower lifetime of the droplets. However, it should also be noted that this parameter is not only dependent on the initial diameter but also dependent on the velocity of the droplet and flame thickness which determines the time spent on each isotherm. In order to include the flame parameters, the critical diameter is also computed from Da_v relation. Calculation with $\bar{K}$, $d_{critical,Da_v}$ overestimates the critical diameter by nearly 2.5 μm due to the minor differences of K for each droplet (46).

4.4. Changes in gaseous properties

From the simulations, changes in gas phase properties are investigated while the droplet is evaporating through the flame field. The focus is made here on the stoichiometric case and initial droplet diameter of 50 μm.

Figure 11 represents the change in ethanol mass fraction, $Y_{C_2H_5OH}$ and reaction source term, $\dot{\omega}_{C_2H_5OH}$ within 1.2 mm distance along x axis which is parallel to the flame, while it is moving perpendicular to flame in y direction. Y coordinates are normalized by the flame thickness so that the comparison can be performed for all conditions. It should also be mentioned that y=0 indicates the flame position, while x=0 points out the centerline of the domain where the ethanol droplet is injected.

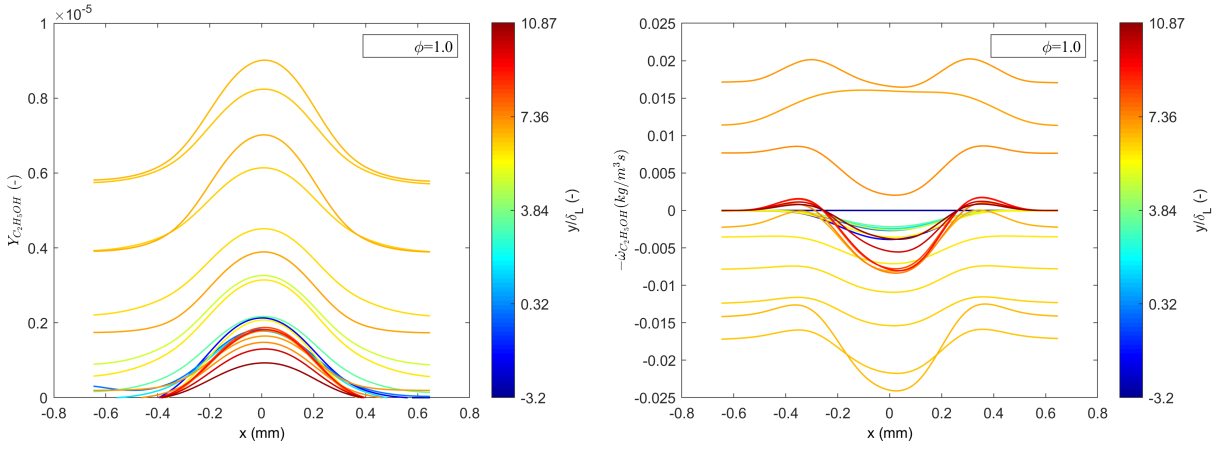

(a) **(b)**

Figure 11: Change in (a) C_2H_5OH mass fraction and (b) C_2H_5OH reaction source term on the isoline of droplet along x axis through the flame at SBM-3

Mass evolution of ethanol in the gas phase can be interpreted from Figure 11a. It is seen that the rate of ethanol build-up in the gas phase increases up to almost 2.8 mm away from the flame, and then, it decreases, although the lifetime of the droplet continues to decline. This trend can also be observed from the mass evaporation rate in Figure 7c. As the droplet closes to the maximum temperature isoline in the gas phase, the surface temperature of the droplet continues to increase. Once the temperature of the droplet becomes constant, the evaporation rate decreases after almost 8 ms at the same distance away from the flame for ϕ=0.9, 1.0, and 1.1. However, for ϕ=0.8, a nearly 2 ms delay is observed at 2.1 mm away from the flame due to the fact that more time is needed for the droplet to reach its boiling temperature at the lowest flame temperature, which is 1991.4 K. Although the velocity of the gases differ at each flame condition, the major effect on gas build-up comes from the flame temperature due to low Stokes number at the performed conditions.

In order to observe the local changes in the reaction zone, the variation of $Y_{C_2H_5OH}$ and $\dot{\omega}_{C_2H_5OH}$ in time on the isoline of the maximum $\dot{\omega}_{CH_4}$ indicating the flame position, is given in Figure 12.

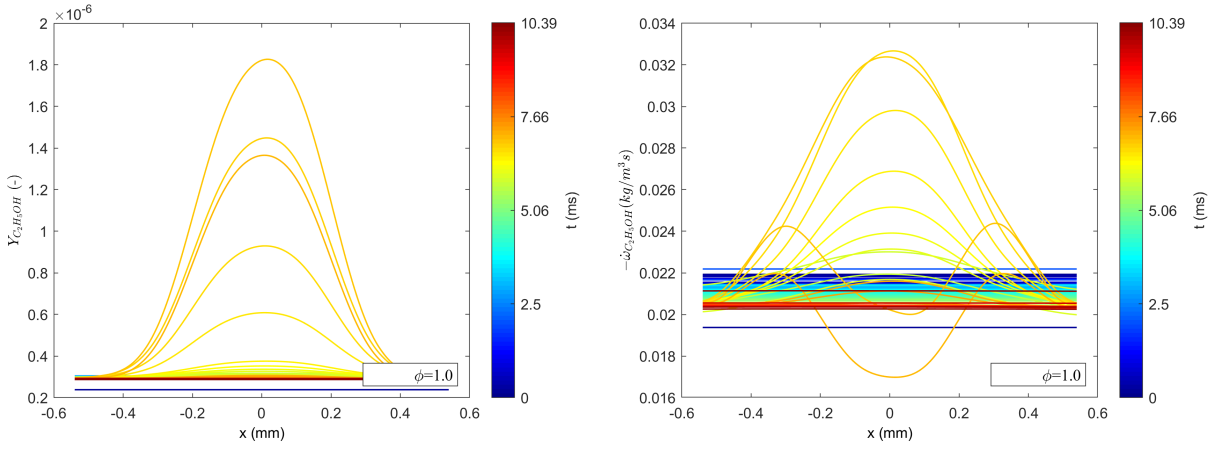

(a) **(b)**

Figure 12: Change in (a) C_2H_5OH mass fraction and (b) C_2H_5OH reaction source term at the flame over time at SBM-3

The prominent increase of ethanol amount in the gas phase is observed between 6-7.5 ms at the flame zone, and then ethanol is consumed. The highest amount of ethanol build-up at the flame is observed for the leanest and richest cases. This phenomenon can be related to the residence time of the droplet by compensating the velocity of the droplet and the flame thickness. Moreover, evaporated ethanol diffuses nearly to 800 μm region on the flame surface, and it increases with the equivalence ratio. Additionally, the droplet takes heat from the flame by decreasing the local temperature nearly by 5 K, expecting to observe a local sink on the flame zone (54).

When the ethanol droplet is vaporized, total fuel concentration increases locally in the flame region. For order of magnitude fuel amount comparison, mass fractions of C_2H_5OH and CH_4 are plotted at the centerline of the domain along the droplet path on y direction, given in Figure 13. The mass fraction of ethanol is multiplied by 10^{-4} to be able to make a comparison with methane.

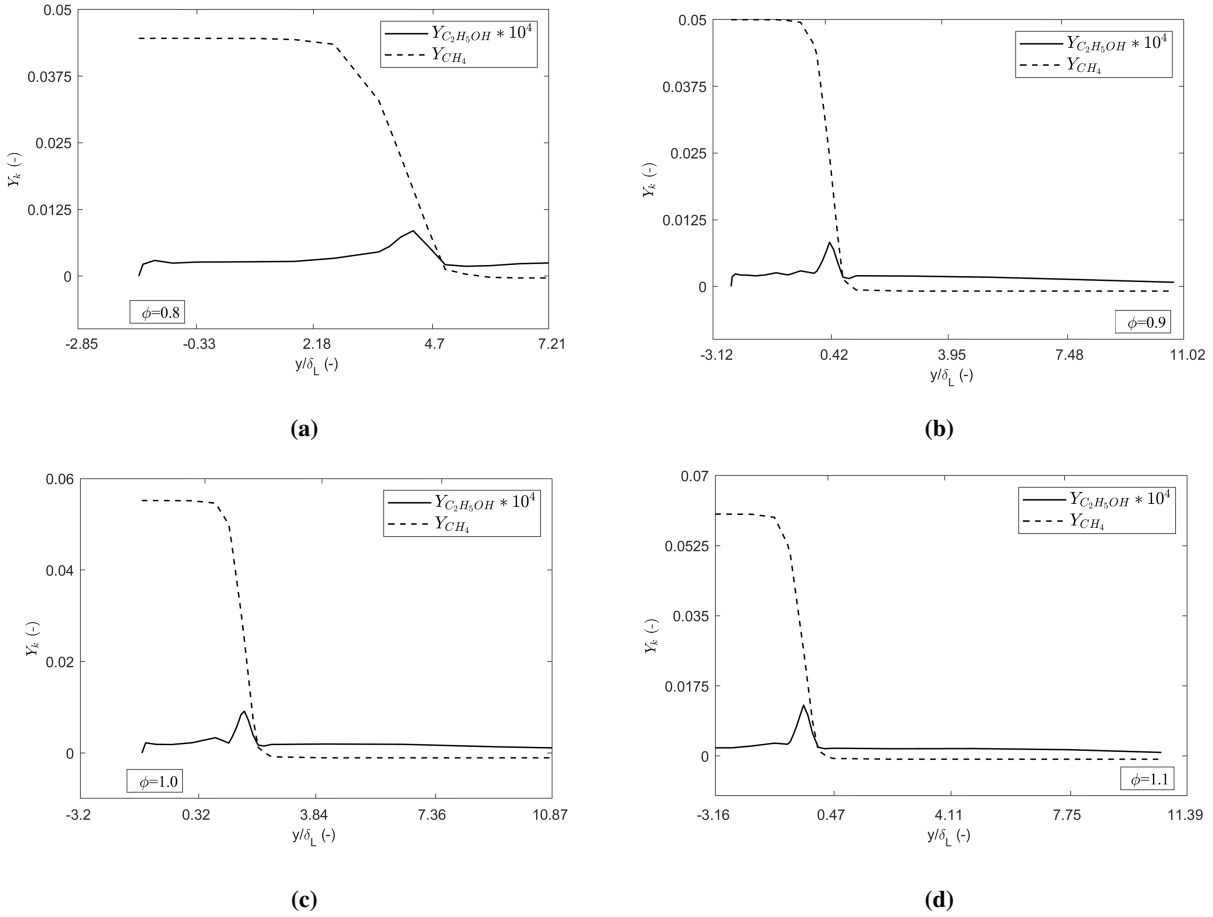

Figure 13: Change in C_2H_5OH and CH_4 mass fractions at the centerline of the domain through the flame

For equal size droplets at different flame conditions, the evaporation rate slightly differs due to the variation of flame temperature, given in Figure 8, which leads to a hardly noticeable difference in gaseous ethanol amount, especially when it is compared with the amount of methane. However, individual comparison gives rise to the reactivity of ethanol in the flame zone. In order to investigate the reactivity of the droplet, reaction source terms of C_2H_5OH and CH_4 are plotted through the droplet path and given in Figure 14.

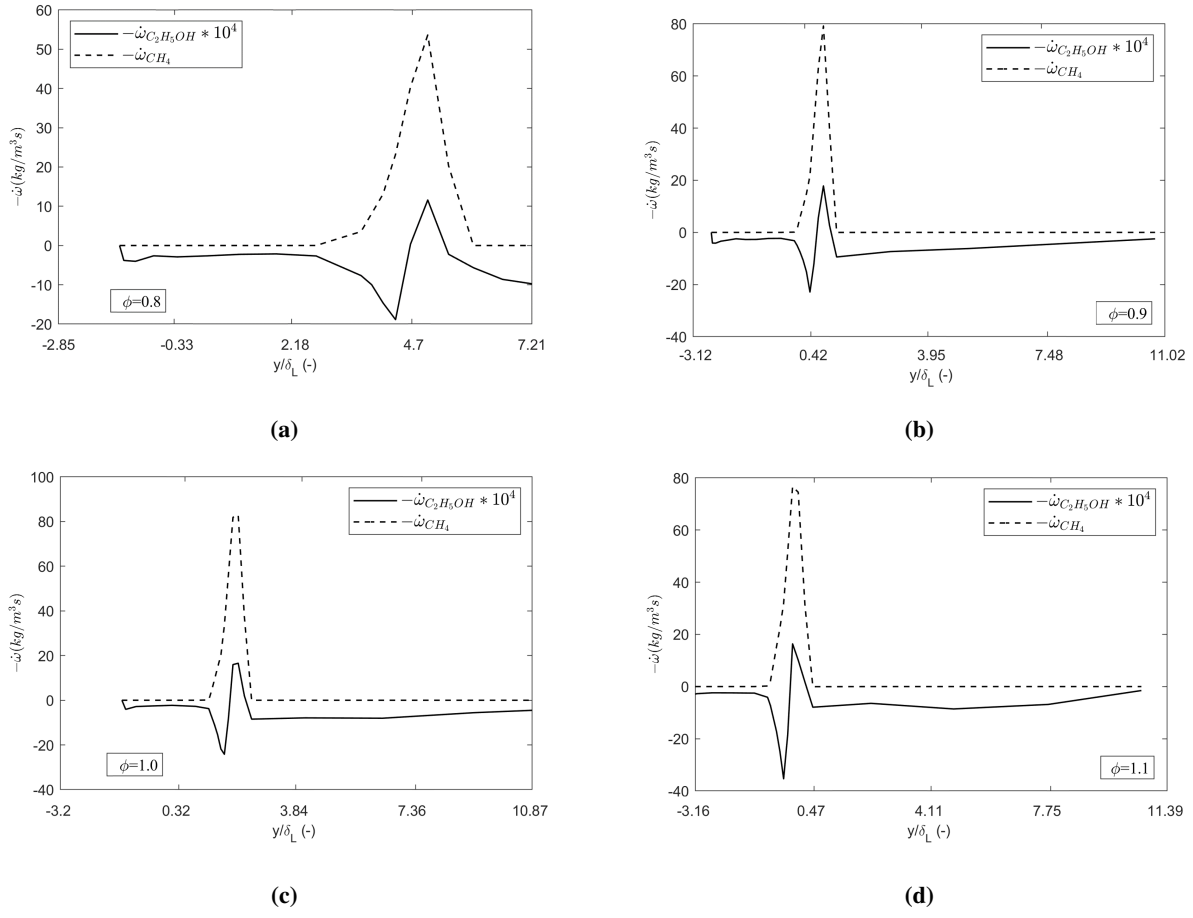

Figure 14: Change in C_2H_5OH and CH_4 reaction source terms at the centerline of the domain through the flame

From the area under positive and negative peaks of ethanol, it can be concluded from Figure 14 that all gaseous ethanol is consumed in the reaction zone, except for the richest case due to the deficiency of excess oxygen at the ambient. Since the gaseous ethanol build-up is high in this case, the expansion of gases is expected to create an extinction on the flame. It should also be mentioned that the mass fractions and source terms of methane and oxygen are not affected noticeably due to the passage of the ethanol droplet since the mass provided to the gaseous phase is nearly negligible when it is compared to gaseous fuel, methane.

4.5. Conclusions

The main objective of this study is to investigate the interaction of a single droplet with a laminar flame and to understand its effects on droplet dynamics and evaporation. The first part of the study includes the experimental investigation of single droplet evaporation in the fuel-rich, stoichiometric and fuel-lean flame conditions. A stagnation burner is utilized to track the droplet evaporation sequence through a stationary premixed laminar flame. An isolated ethanol droplet having nearly 50 μm initial diameter is injected through methane/air stagnation flames . The motion of the droplet and velocity of the unburnt gases are tracked via PTV and PIV, respectively. Simultaneously, the change in diameter of the droplet is tracked via ILIDS. Simulations are performed with different configurations, including stationary droplet evaporation surrounded by burnt gases at the flame conditions, the injection of an ethanol droplet to the stagnation flame field, and more realistic flame conditions with the real burner geometry. The whole sequence of droplet evaporation is tracked, and the properties of the droplet is computed using Lagrangian evaporation models, including Spalding and Abramzon-Sirignano models.

The flame temperature is found to be the most dominant effect on the evaporation rate rather than the burnt gas composition and flame strain rate. Additionally, the evaporation constant is computed to be almost insensitive to

the initial droplet diameter. Mean evaporation temperature is reported for the droplet passing through a temperature gradient, and the average evaporation rate is determined between 0.5-0.7 mm^2/s. The evaporation rate is also expressed empirically as an exponential function of flame parameters, and it is found to be slightly dependent on the flame speed and flame thickness. The critical diameter of an ethanol droplet is calculated to be nearly 20 μm indicating that a larger droplet can cross the flame region and cause local modifications. From the gas phase change, it is observed that all evaporated ethanol reacts with oxygen in the flame zone, except from ϕ=1.1, due to the lack of excess oxygen in the gaseous phase for methane/air flames. The heat is taken by the evaporating droplet in the flame zone, and the vaporized ethanol diffuses nearly to 800 μm along the flame for $d_{p,0}$=50 μm.

Declaration of Competing Interest

The authors declare that they have no known competing financial interests or personal relationships that could have appeared to influence the work reported in this paper.

Acknowledgments

The authors acknowledge CNES for its financial support and CNRS CORIA for permitting the use of YALES2 code, special thanks to Dr. Vincent Moureau for his guidance. DKE is financially supported by French Government Cotutelle Scholarship for her joint PhD studies between METU & Université d'Orléans and TÜBİTAK BİDEB 2211-C Scholarship.

References

[1] M. Birouk, I. Gokalp, Current status of droplet evaporation in turbulent flows, Prog. Energ. Combust. 32 (2006) 408–423.
[2] V. Raghavan, Numerical modeling of evaporation and combustion of isolated liquid fuel droplets: A review, J. Indian I. Sci. 99 (2019) 5–23.
[3] S. S. Sazhin, Modelling of fuel droplet heating and evaporation: Recent results and unsolved problems, Fuel 196 (2017) 69–101.
[4] Z. Wang, B. Yuan, Y. Huang, J. Cao, Y. Wang, X. Cheng, Progress in experimental investigations on evaporation characteristics of a fuel droplet, Fuel Process. Technol. 231 (2022) 107243.
[5] Z. Zhifu, W. Guoxiang, C. Bin, G. Liejin, W. Yueshe, Evaluation of evaporation models for single moving droplet with a high evaporation rate, Powder Technol. 240 (2013) 95–102.
[6] Y. Zhang, S. Li, B. Lin, Y. Liu, J. Wu, B. Xu, A review on laser diagnostics on atomization and evaporation of liquid fuel, Proc. Spie. (2014) 923202.
[7] H. Ghassemi, S. W. Baek, Q. S. Khan, Experimental study on binary droplet evaporation at elevated pressures and temperatures, Combust. Sci. Technol. 178 (2006) 1031–1053.
[8] J. Wang, X. Huang, X. Qiao, D. Ju, C. Sun, Experimental study on effect of support fiber on fuel droplet vaporization at high temperatures, Fuel 268 (2020) 117407.
[9] S. Kumagai, T. Sakai, S. Okajima, Combustion of free fuel droplets in a freely falling chamber, Symp. (Int.) Combust. 13 (1971) 779–785.
[10] J. Stengele, K. Prommersberger, M. Willmann, S. Wittig, Experimental and theoretical study of one- and two-component droplet vaporization in a high pressure environment, Int. J. Heat Mass Tran. 42 (1999) 2683–2694.
[11] G. Brenn, L. J. Deviprasath, F. Durst, C. Fink, Evaporation of acoustically levitated multi-component liquid droplets, Int. J. Heat Mass Tran. 50 (2007) 5073–5086.
[12] H. Grosshans, M. Griesing, M. Mönckedieck, T. Hellwig, B. Walther, S. R. Gopireddy, R. Sedelmayer, W. Pauer, H.-U. Moritz, N. A. Urbanetz, E. Gutheil, Numerical and experimental study of the drying of bi-component droplets under various drying conditions, Int. J. Heat Mass Tran. 96 (2016) 97–109.
[13] C. Espey, J. E. Dec, T. A. Litzinger, D. A. Santavicca, Quantitative 2-D fuel vapor concentration imaging in a firing D.I. diesel engine using planar laser-induced Rayleigh scattering, SAE Transactions 103 (1994) 1145–1160.
[14] A. Adam, P. Leick, G. Bittlinger, C. Schulz, Visualization of the evaporation of a diesel spray using combined Mie and Rayleigh scattering techniques, Exp. Fluids 47 (2009) 439–449.
[15] C. Maqua, G. Castanet, F. Lemoine, Bicomponent droplets evaporation: Temperature measurements and modelling, Fuel 87 (2008) 2932–2942.
[16] P. A. Strizhak, R. S. Volkov, G. Castanet, F. Lemoine, O. Rybdylova, S. S. Sazhin, Heating and evaporation of suspended water droplets: Experimental studies and modelling, Int. J. Heat Mass Tran. 127 (2018) 92–106.
[17] A. Verdier, J. Marrero Santiago, A. Vandel, S. Saengkaew, G. Cabot, G. Grehan, B. Renou, Experimental study of local flame structures and fuel droplet properties of a spray jet flame, Proc. Combust. Inst. 36 (2017) 2595–2602.
[18] C. Schulz, V. Sick, Tracer-LIF diagnostics: Quantitative measurement of fuel concentration, temperature and fuel/air ratio in practical combustion systems, Prog. Energ. Combust. 31 (2005) 75–121.
[19] M. C. Thurber, F. Grisch, R. K. Hanson, Temperature imaging with single- and dual-wavelength acetone planar laser-induced fluorescence, Opt. Lett. 22 (1997) 251–253.
[20] L. A. Melton, Spectrally separated fluorescence emissions for diesel fuel droplets and vapor, Appl. Optics 22 (1983) 2224–2226.
[21] P. Lavieille, F. Lemoine, G. Lavergne, M. Lebouché, Evaporating and combusting droplet temperature measurements using two-color laser-induced fluorescence, Exp. Fluids 31 (2001) 45–55.

[22] G. Castanet, P. Lavieille, M. Lebouché, F. Lemoine, Measurement of the temperature distribution within monodisperse combusting droplets in linear streams using two-color laser-induced fluorescence, Exp. Fluids 35 (2003) 563–571.
[23] K. T. Kobayashi, T., M. Maeda, Measurement of spray flow by an improved Interferometric Laser Imaging Droplet Sizing (ILIDS) system, in: R. J. Adrian, D. F. G. Durao, M. V. Heitor, M. Maeda, C. Tropea, J. H. Whitelaw (Eds.), Laser Techniques for Fluid Mechanics, Berlin, 2002, pp. 209–220.
[24] S. Sahu, Y. Hardalupas, A. M. K. P. Taylor, Simultaneous droplet and vapour-phase measurements in an evaporative spray by combined ILIDS and PLIF techniques, Exp. Fluids 55 (2014) 1673.
[25] S. Sahu, Y. Hardalupas, A. M. K. P. Taylor, Interaction of droplet dispersion and evaporation in a polydispersed spray, J. Fluid Mech. 846 (2018) 37–81.
[26] G. Parant, L. Zimmer, A. Renaud, F. Richecoeur, Adaptation of a PTV method for droplets evaporating in vicinity of a flame, Exp. Fluids 63 (2022) 100.
[27] D. B. Spalding, Combustion of liquid fuels, Nature 165 (1950) 160–160.
[28] G. Godsave, Studies of the combustion of drops in a fuel spray—the burning of single drops of fuel, Symp. (Int.) Combust. 4 (1953) 818–830.
[29] W. Ranz, J. Marshall, Wr: Evaporation from drops, Chem. Eng. Prog. 48 (1952) 141–146.
[30] B. Abramzon, W. A. Sirignano, Droplet vaporization model for spray combustion calculations, Int. J. Heat Mass Tran. 32 (1989) 1605–1618.
[31] S. Sazhin, W. Abdelghaffar, E. Sazhina, M. Heikal, Models for droplet transient heating: Effects on droplet evaporation, ignition, and break-up, Int. J. Therm. Sci. 44 (2005) 610–622.
[32] R. Haywood, R. Nafziger, M. Renksizbulut, A detailed examination of gas and liquid phase transient processes in convective droplet evaporation, J. Heat Transf. 111 (1989) 495–502.
[33] R. Miller, K. Harstad, J. Bellan, Evaluation of equilibrium and non-equilibrium evaporation models for many-droplet gas-liquid flow simulations, Int. J. Multiphas. Flow 24 (1998) 1025–1055.
[34] A. Verdier, J. M. Santiago, A. Vandel, G. Godard, G. Cabot, B. Renou, Local extinction mechanisms analysis of spray jet flame using high speed diagnostics, Combust. Flame 193 (2018) 440–452.
[35] D. Paulhiac, B. Cuenot, E. Riber, L. Esclapez, S. Richard, Analysis of the spray flame structure in a lab-scale burner using Large Eddy Simulation and Discrete Particle Simulation, Combust. Flame 212 (2020) 25–38.
[36] M. Bonanni, M. Ihme, Interaction of preferential evaporation and low-temperature chemistry in multicomponent counterflow spray flames, Proc. Combust. Inst. 39 (2023) 2565–2573.
[37] L. Fan, B. Tian, C. T. Chong, M. N. M. Jaafar, K. Tanno, D. McGrath, P. M. de Oliveira, B. Rogg, S. Hochgreb, The effect of fine droplets on laminar propagation speed of a strained acetone-methane flame: Experiment and simulations, Combust. Flame 229 (2021) 111377.
[38] B. Rochette, E. Riber, B. Cuenot, Effect of non-zero relative velocity on the flame speed of two-phase laminar flames, Proc. Combust. Inst. 37 (2019) 3393–3400.
[39] J. Sangiovanni, M. Labowsky, Burning times of linear fuel droplet arrays: A comparison of experiment and theory, Combust. Flame 47 (1982) 15–30.
[40] S. Russo, A. Gomez, The extinction behavior of small interacting droplets in cross-flow, Combust. Flame 130 (2002) 215–224.
[41] S. Russo, A. Gomez, Structure of laminar coflow spray flames at different pressures, Proc. Combust. Inst. 29 (2002) 601–608.
[42] G. Castanet, M. Lebouché, F. Lemoine, Heat and mass transfer of combusting monodisperse droplets in a linear stream, Int. J. Heat Mass Tran. 48 (2005) 3261–3275.
[43] M. Orain, Y. Hardalupas, Droplet characteristics and local equivalence ratio of reacting mixture in spray counterflow flames, Exp. Therm. Fluid Sci. 57 (2014) 261–274.
[44] X. Mercier, M. Orain, F. Grisch, Investigation of droplet combustion in strained counterflow diffusion flames using planar laser-induced fluorescence, Appl. Phys. B-Lasers O. 88 (2007) 151–160.
[45] D. Kaya, G. Renoux, F. Halter, A. Yozgatligil, I. Gokalp, C. Chauveau, Evaporation of a single ethanol droplet interacting with a premixed laminar CH_4/air flame, 15th Triennial International Conference on Liquid Atomization and Spray Systems (2021).
[46] D. Kaya Eyice, G. Renoux, F. Halter, A. Yozgatligil, I. Gokalp, C. Chauveau, Vaporization characteristics of an isolated ethanol droplet at flame conditions, Atomization Spray. 32 (2022).
[47] D. G. Goodwin, R. L. Speth, H. K. Moffat, B. W. Weber, Cantera: An object-oriented software toolkit for chemical kinetics, thermodynamics, and transport processes, 10.5281/ZENODO.1174508, accessed: 09.25.2023 (2018).
[48] Chemical-kinetic mechanisms for combustion applications, San Diego Mechanism, Mechanical and Aerospace Engineering (Combustion Research), University of California at San Diego, http://combustion.ucsd.edu, accessed: 09.25.2023 (2016).
[49] V. Moureau, P. Domingo, L. Vervisch, Design of a massively parallel CFD code for complex geometries, CR. Mécanique 339 (2011) 141–148.
[50] Z. Naumann, L. Schiller, A drag coefficient correlation, Z. Ver. Deutsch. Ing 77 (1935) e323.
[51] G. L. Hubbard, V. E. Denny, A. F. Mills, Droplet evaporation: Effects of transients and variable properties, Int. J. Heat Mass Tran. 18 (1975) 1003–1008.
[52] G. Renoux, F. Halter, C. Chauveau, Experimental study of the morphology of two-phase flame instabilities in microgravity, Atomization Spray. 28 (2018).
[53] S. B. Saharin, B. Lefort, C. Morin, C. Chauveau, L. L. Moyne, R. Kafafy, Vaporization characteristics of ethanol and 1-propanol droplets at high temperatures, Atomization Spray. 22 (2012).
[54] D. Kaya Eyice, F. Halter, A. Yozgatligil, I. Gokalp, C. Chauveau, Investigation of cellular instabilities and local extinction for two-phase flames under microgravity conditions, CR. Mécanique 351 (2023) 1–16.
[55] J. Reveillon, Direct numerical simulation of sprays: Turbulent dispersion, evaporation and combustion, in: Multiphase Reacting Flows: Modelling and Simulation, Vienna, 2007, pp. 229–269.